Band structure, Fermi surface, elastic, thermodynamic, and optical properties of $AlZr_3$, $AlCu_3$, and $AlCu_2Zr$: First-principles study

Parvin R[1], Parvin F[1], Ali M S[2,†], and Islam A K M A[3]

[1] *Department of Physics, Rajshahi University, Rajshahi-6205, Bangladesh*
[2] *Department of Physics, Pabna University of Science and Technology, Pabna 6600, Bangladesh*
[3] *International Islamic University Chittagong, 154/A College Road, Chittagong-4203, Bangladesh*

(Received 10 October 2015; revised manuscript received 4 April 2016; published online 25 June 2016)

The electronic properties (Fermi surface, band structure, and density of states (DOS)) of Al-based alloys AlM_3 (M = Zr and Cu) and $AlCu_2Zr$ are investigated using the first-principles pseudopotential plane wave method within the generalized gradient approximation (GGA). The structural parameters and elastic constants are evaluated and compared with other available data. Also, the pressure dependences of mechanical properties of the compounds are studied. The temperature dependence of adiabatic bulk modulus, Debye temperature, specific heat, thermal expansion coefficient, entropy, and internal energy are all obtained for the first time through quasi-harmonic Debye model with phononic effects for $T = 0$ K–100 K. The parameters of optical properties (dielectric functions, refractive index, extinction coefficient, absorption spectrum, conductivity, energy-loss spectrum, and reflectivity) of the compounds are calculated and discussed for the first time. The reflectivities of the materials are quite high in the IR–visible–UV region up to $\sim$ 15 eV, showing that they promise to be good coating materials to avoid solar heating. Some of the properties are also compared with those of the Al-based Ni_3Al compound.

Keywords: first principle calculations, Fermi surface, elastic moduli, entropy, and internal energy, optical properties

PACS: 31.15.A–, 71.18.+y, 62.20.de, 65.40.gd **DOI:** 10.1088/1674-1056/25/8/083101

1. Introduction

Aluminum-based alloys have received much attention in recent years because of their important roles in many technological applications. They have vast applications in the aerospace, microelectronic, motorized vehicles, and domestic industry. As the alloys are important in the engineering and research areas, mechanical behavior has become a focus of various investigations. A large quantity of alloy elements can be used to form the Al-based intermetallic compounds. It is observed that the bonding behaviors and electronic natures are changed of such a type of alloys which show excellent mechanical, physical, and chemical properties.[1] The compounds involving aluminum and transition metals are known to have high resistance to oxidation and corrosion, elevated-temperature strength, relatively low density, and high melting points, which make them desirable candidates for high-temperature structural applications.[2] Zirconium can effectively enhance the mechanical strengths of the alloys when copper and zinc elements exist in aluminum and Al-based alloys.[3] Many investigations have focused on the constituent binary systems, such as Al–Cu, Al–Zr, and Cu–Zr.[4–9] Some theoretical investigations have been performed on Al-based alloys such as structural, elastic and electronic properties.[10,11]

To the best of our knowledge, electronic band structures, Fermi surfaces, thermal and optical properties of $AlZr_3$, $AlCu_3$, and $AlCu_2Zr$ compounds have not yet been discussed theoretically and experimentally. The thermodynamic properties include a variety of properties and phenomena such as bulk modulus, specific heat, thermal expansion coefficient, Debye temperature, etc. The specific heat of a material is one of the most important thermodynamic properties indicating its heat retention or loss ability. We have also briefly discussed our calculated structural and elastic properties for $AlZr_3$, $AlCu_3$, and $AlCu_2Zr$ intermetallic alloys.

On the other hand, the optical properties of solids provide an important tool for studying energy band structures, impurity levels, localized defects, lattice vibrations, and certain magnetic excitations. The optical conductivity or the dielectric function indicates a response of a system of electrons to an applied field. Thus there is a need to deal with all these issues which have been covered for the first time in the present paper. A detailed discussion and analysis are made, some of which are in comparison with the results of available Al-based alloys.[10,12]

2. Computational details

The density functional theory (DFT) based on the CASTEP code has been used in the present investi-

†Corresponding author. E-mail: shahajan199@yahoo.com

© 2016 Chinese Physical Society and IOP Publishing Ltd

gation.[13–16] The interactions between valence electrons and ions are considered using the ultrasoft pseudopotential formalism of Vanderbilt.[17] To find out the minimum potential energy of the compound, a quasi-Newton (variable-metric) minimization method, the Broyden–Fletcher–Goldfarb–Shanno (BFGS) update scheme,[18] is utilized, which provides a very efficient and fast way to explore the optimizing crystal structure. The electron wave function is expanded in plane waves up to an energy cutoff of 400 eV for $AlZr_3$ and 500 eV for $AlCu_3$ as well as $AlCu_2Zr$ for the sampling of the Brillouin zone,[19] a $15\times15\times15$, $21\times21\times21$, $9\times9\times9$ Monkhorst–Pack mesh are employed[20] for $AlZr_3$, $AlCu_3$, and $AlCu_2Zr$, respectively. Generalized gradient approximation (GGA) of the Perdew–Burke–Ernzerhof for solids (PBEsol) formalism,[16] which is dependent on both the electron density and its gradient at each space point is used to evaluate the exchange-correlation energy. Optimization is performed using a convergence threshold of 10^{-5} eV/atom for the total energy and 10^{-3} Å for maximum displacement. Maximum force and stress are 0.03 eV/Å and 0.05 GPa, respectively for all the calculations. Norm conserving pseudopotential is used only for calculating the optical properties, keeping the other setup unchanged. The resulting stress can be calculated with respect to the optimized crystal structure[21] using a set of homogeneous deformations with a finite value.

The thermodynamic properties are studied within the quasi-harmonic Debye model implemented in the Gibbs program,[22] a detailed description of which can be found in Refs. [23]–[25]. We use the DFT calculated $E\sim V$ (energy $\sim$ volume) data at $T=0$ K, $P=0$ GPa, and the third-order Birch–Murnaghan EOS.[26] Using this, the thermodynamic properties such as the bulk modulus, thermal expansion coefficient, specific heats, and Debye temperature at non-zero temperature and pressure are calculated.

3. Results and discussion

3.1. Structural properties

Aluminum-based intermetallic AlM_3 (M =Zr and Cu) binary alloys crystallize into the cubic Cu_3Au structure[27,28] with space group Pm-3m (No. 221) consisting of Al atoms at the corners and M atoms at the face centers of the cube. The atomic positions are Al: 1a $(0,0,0)$, and M: 3c $(0,1/2,1/2)$. The ternary $AlCu_2Zr$ alloy is a partially ordered Cu_2MnAl-type fcc (space group No. 225: Fm-3m) structure,[29] where Al atoms occupy the 4a Wyckoff site $(0,0,0)$, Cu atoms occupy the 8c site $(1/4,1/4,1/4)$ and Zr atoms occupy the 4b site $(1/2,1/2,1/2)$. In order to investigate the ground-state properties of AlM_3 (M =Zr and Cu) and $AlCu_2Zr$ alloys, the geometry optimizations are performed first with the full relaxation of the cell shape and atomic positions. The equilibrium crystal structures of these compounds are shown in Fig. 1. The results of first-principles calculations of the structural properties of these compounds are presented in Table 1, together with the available experimental values[27–29] and other theoretical results.[10] The comparison shows that our results are in reasonable agreement with both theoretical and experimental values.

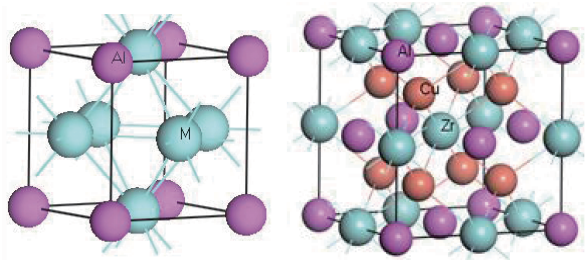


Fig. 1. (color online) Crystal structures of AlM_3 (M =Zr and Cu) and $AlCu_2Zr$.

Table 1. Values of calculated and experimental lattice constant a (in unit Å), equilibrium volume V_0 (in units Å^3), bulk modulus B_0 (in unit GPa) of $AlZr_3$, $AlCu_3$, and $AlCu_2Zr$ alloys.

Compounds	a	V_0	B_0	Ref.
$AlZr_3$	4.3799	84.02	99.2	this paper
	4.381	84.11	100.8	[10]
	4.392	84.70	–	[27]
$AlCu_3$	3.6909	50.28	129.0	this paper
	3.693	50.36	131.0	[10]
	3.607	–	–	[28]
$AlCu_2Zr$	6.2525	244.43	129.4	this paper
	6.256	244.81	128.6	[10]
	6.216	240.21	–	[29]

3.2. Mechanical properties

Generally, elastic constants of a solid permit us to obtain the mechanical properties and they can be used to describe the resistance of a crystal to an externally applied stress. They also provide important information about bonding characteristics near the equilibrium state. Thus, it is essential to investigate the elastic constants to understand the mechanical behavior of AlM_3 (M =Zr and Cu) and $AlCu_2Zr$ compounds at equilibrium and under pressure. For a material with cubic symmetry, there are only three independent elastic constants, i.e., C_{11}, C_{12}, and C_{44}. In this paper, the calculated single crystal elastic constants of these compounds are listed in Table 2. It can be seen that the obtained elastic constants of the alloys agree well with the theoretical results in Ref. [10], which indicates that the DFT method we used in this study is reasonable. Furthermore, the corresponding requirements of mechanical stability in a cubic crystal lead to the following restriction on the elastic constants:[30] $C_{11}+2C_{12}>0$, $C_{44}>0$, $C_{11}-C_{12}>0$. As shown in Table 2, all of the elastic constants for the compounds satisfy these criteria mentioned above, indicating that these compounds are mechanically stable.

Table 2. Values of calculated elastic constants C_{ij} (in unit GPa), bulk modulus B (in unit GPa), shear modulus G (in unit GPa), Young's modulus E (in unit GPa), Poisson's ratio ν, elastic anisotropic factor A for $AlZr_3$, $AlCu_3$, and $AlCu_2Zr$ alloys at equilibrium.

Compound	C_{11}/GPa	C_{12}/GPa	C_{44}/GPa	B/GPa	G/GPa	E/GPa	B/G	ν	A	Ref.
$AlZr_3$	147.4	75.2	74.2	99.2	55.6	140.5	1.78	0.264	1.52	this paper
	148.7	79.4	70.8	102.5	53.4	136.5	1.92	0.278	1.49	[10]
	163.8	79.3	86.5	107.7	–	–	–	–	–	[5]
$AlCu_3$	152.4	117.3	85.4	129.0	45.9	123.1	2.81	0.341	1.89	this paper
	150.7	120.6	81.9	130.6	43.6	117.7	3.00	0.350	1.89	[10]
	176.0	117.4	92.4	136.9	49.6	132.8	–	0.340	–	[4]
$AlCu_2Zr$	180.6	103.8	65.7	129.4	53.0	139.9	2.44	0.320	1.30	this paper
	157.5	115.3	62.7	129.4	41.2	111.8	3.14	0.356	1.53	[10]

The pressure dependences of the calculated elastic constants of $AlZr_3$, $AlCu_3$, and $AlCu_2Zr$ are plotted in Fig. 2. The linear increases of elastic constants are due to the decreases of lattice parameters of all the compounds under pressure (not shown). It is noticeable that C_{11} increases more rapidly with pressure than C_{12} and C_{44}. C_{11} represents elasticity in the x direction, i.e., in length, the longitudinal strain produces a significant change in volume. Again, the volume change is highly related to the pressure and thus produces a large change in C_{11}. Conversely, the constants C_{12} and C_{44} are related to the elasticity in shape.

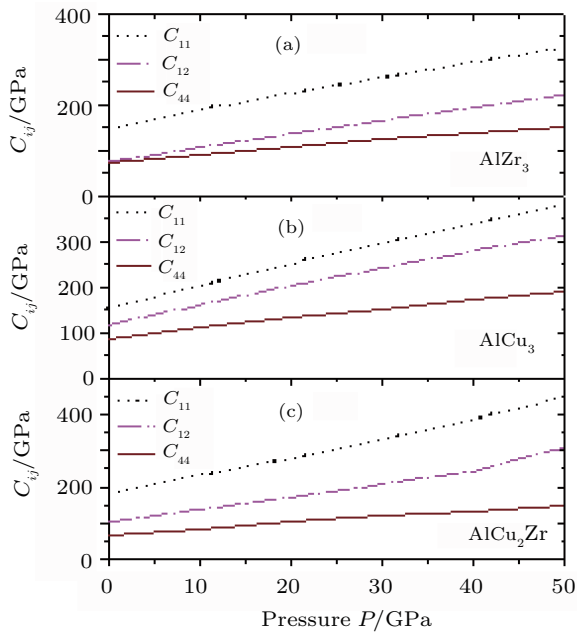


Fig. 2. (color online) Pressure dependences of elastic constants of (a) $AlZr_3$, (b) $AlCu_3$, and (c) $AlCu_2Zr$.

The polycrystalline elastic properties, such as bulk modulus B, shear modulus G, Young's modulus E, and Poisson's ratio ν are estimated from the calculated single crystal elastic constants, and are presented in Table 2. The calculated results show that G for $AlZr_3$ is the largest, while for $AlCu_2Zr$ it is less than that for $AlCu_3$, which agrees well with the available theoretical calculation.[10]

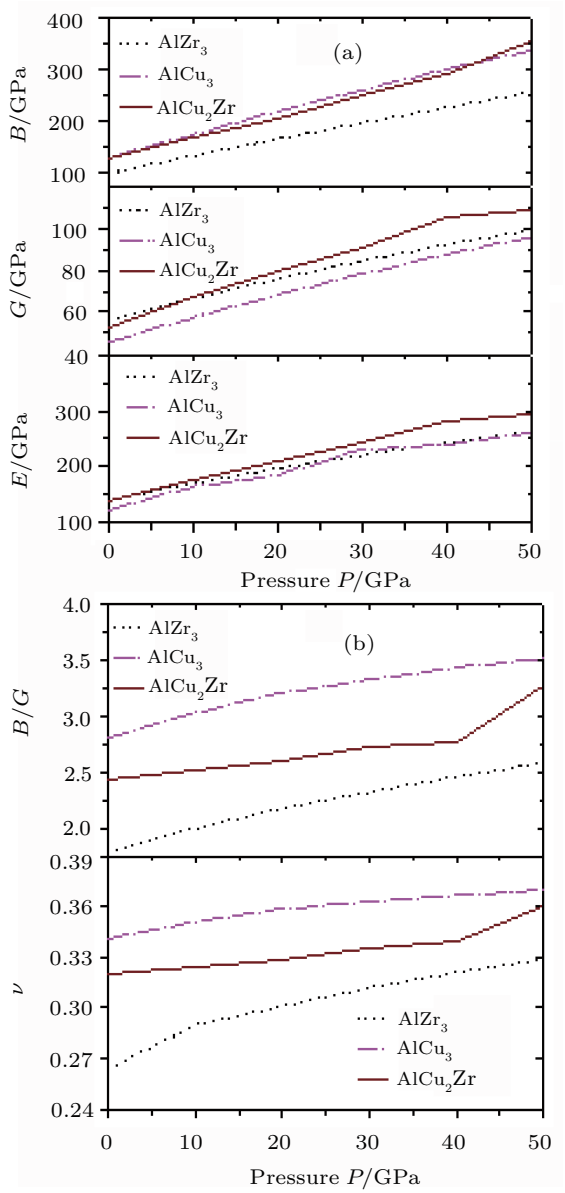


Fig. 3. (color online) Pressure effects on (a) bulk modulus (B), shear modulus (G), and Young's modulus (E); (b) the values of ratio of bulk modulus to shear modulus (B/G) and Poisson's ratio (ν) of $AlZr_3$, $AlCu_3$, and $AlCu_2Zr$.

The pressure effects on the calculated bulk modulus, shear modulus, and Young's modulus of $AlZr_3$, $AlCu_3$, and $AlCu_2Zr$ are shown in Fig. 3(a). The rate of increase of G

with pressure is smaller than those of B and E. The shear modulus G is mainly due to the elastic constant C_{44}, because a large C_{44} implies a stronger resistance to shear in the (100) plane. Young's moduli of $AlZr_3$ and $AlCu_2Zr$ are nearly equal at $P = 0$ GPa but when pressure increases the Young's modulus for $AlCu_2Zr$ increases more rapidly than those for the other two phases, which indicates that $AlCu_2Zr$ phase is much stiffer than the other two phases at high pressure.

Figure 3(b) shows the pressure dependences of Poisson's ratio and B/G of $AlZr_3$, $AlCu_3$, and $AlCu_2Zr$. Poisson's ratio can reflect the bonding properties of material. For the different bonding materials, Poisson's ratios are different.[31] As for a covalent material, the value of ν is small (typically ~ 0.1); for an ionic material, the typical value of ν is 0.25; for a metallic material, ν is typically 0.33.[31] In this case, Poisson's ratio ranges from 0.264 to 0.341, which indicates that the AlM_3 (M = Zr and Cu) and $AlCu_2Zr$ compounds show metallic behaviors. Poisson's ratio increases with pressure increasing, the larger Poisson's ratio signifies better plasticity. Hence it can be said that $AlCu_3$ possesses better plasticity than the other two phases. Additionally, in order to evaluate the ductility of material, a parameter B/G has been proposed by Pugh.[32] The critical value separating ductility from brittleness is about 1.75. In the present work, the calculated values of B/G (Table 2) for these three compounds are all higher than 1.75, implying that AlM_3 (M = Zr and Cu) and $AlCu_2Zr$ alloys behave in a ductile manner. Figure 3(b) shows that B/G increases with pressure growing for all the compounds under study. It indicates that $AlZr_3$, $AlCu_3$, and $AlCu_2Zr$ are ductile compounds at up to 50 GPa. Anisotropy is used to describe situations where properties vary systematically, dependent on the direction. $A = 2C_{44}/(C_{11} - C_{12})$ is called a shear anisotropy factor, often used to represent the elastic anisotropy of crystals.[33] The A values of 1.52, 1.89, and 1.30 for AlM_3 (M = Zr and Cu) and $AlCu_2Zr$ alloys, respectively quantify elastic anisotropies. It is noted that $AlCu_3$ phase is much more anisotropic than the other two phases.

3.3. Electronic band structure and Fermi surface

The investigated electronic band structures along high symmetry directions in the Brillouin zones together with the total densities of states (DOSs) of $AlZr_3$, $AlCu_3$, and $AlCu_2Zr$ are depicted in Fig. 4. The band structures reveal metallic characters with dispersion bands crossing the Fermi level (E_F) for all structures. For $AlZr_3$ and $AlCu_2Zr$ alloys, Zr 4d orbitals are mainly responsible for the metallic characters. But for $AlCu_3$, at the Fermi level, the main contribution comes from the Cu 3d orbitals.

It is observed from Fig. 4(a) that for $AlZr_3$ alloy, the hybridization between Al 3p orbital and Zr 4d orbital is strong both below and above the Fermi level. For this reason the entire DOS can be divided into bonding and anti-bonding regions and therefore a pseudogap resides in between. The characteristic pseudogap around the Fermi level indicates the presence of the directional covalent bonding. The Fermi level located at a valley in the bonding region implies that the system has a pronounced stability.[10] There is a general consideration that the formation of covalent bonding would enhance the strength of material in comparison with the pure metallic bonding.[34]

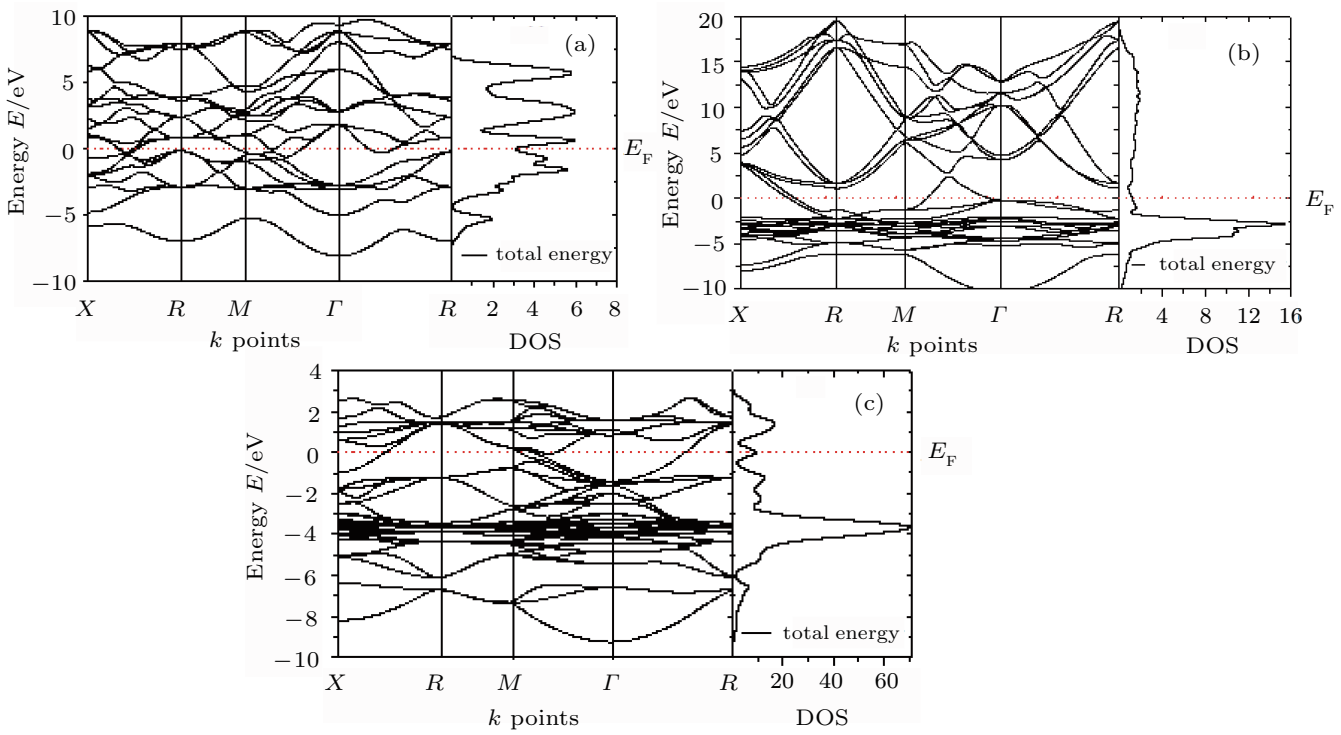


Fig. 4. Band structures and total DOSs of (a) $AlZr_3$, (b) $AlCu_3$, and (c) $AlCu_2Zr$.

According to the covalent approach, the guiding principle is to maximize bonding. Hence the stability increases with increasing occupancy in the bonding region, for a series of compounds having the same structure.[35] Therefore it can be said that $AlZr_3$ is structurally more stable than $AlCu_3$. On the other hand, for $AlCu_2Zr$, the main bonding peaks from Fermi level to 3 eV predominantly derive from the Zr 4d orbitals. The phase stability of intermetallic compound depends on the location of the Fermi level and the value of the DOS at E_F.[36,37] The lower value of DOS at E_F corresponds to a more stable structure. The values of the total DOS at the Fermi level in states are 3.2 eV and 9.3 eV for $AlZr_3$ and $AlCu_2Zr$ alloys, respectively. Therefore, it can be said that $AlZr_3$ has a more stable structure than the other two alloys of Al under consideration, which agrees very well with the observation in Ref. [10].

The shape of the Fermi surface is derived from the periodicity and symmetry of the crystalline lattice and from the occupation of electronic energy bands. It separates unfilled orbitals from the filled orbitals. The Fermi surface topologies of $AlZr_3$, $AlCu_3$, and $AlCu_2Zr$ are shown in Fig. 5. The shapes of the Fermi surfaces are quite different for the three Al-based intermetallic compounds. In the cases of $AlZr_3$ and $AlCu_3$, two energy bands cross the Fermi level. They form two Fermi sheets. $AlZr_3$ has a hole-like Fermi surface around R point as well as around X point. The topology of the Fermi surface of $AlZr_3$ is nearly similar to that of YPb_3.[38] Again, $AlCu_3$ has two hole-like Fermi sheets around X point. On the other hand, $AlCu_2Zr$ alloy has four Fermi sheets because four energy bands cross the Fermi level. The topology of this Fermi surface is complicated; it has hole-like sheets around R point and electron-like sheets around Γ point.

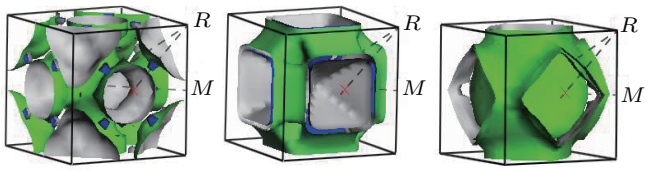


Fig. 5. (color online) Fermi surfaces of (a) $AlZr_3$, (b) $AlCu_3$, and (c) $AlCu_2Zr$.

Charge transport is mainly limited by carrier–carrier and carrier–phonon scattering. Besides, there is always impurity scattering in most real systems. The carrier–carrier scattering is intimately related to the electronic band structure and density of states at the Fermi level. The topology of the Fermi surface also plays a role. For example, the highly dispersive nature of energy dispersion curve for $AlZr_3$ (Fig. 4(a)) around the Fermi energy, implies high carrier mobility. This is supported by the large low energy optical conductivity seen in Fig. 11(h) for the same compound ($AlZr_3$).

3.4. Thermal properties

The thermodynamic properties such as the bulk moduli, specific heats, Debye temperatures, and volume thermal expansion coefficients at different temperatures and pressures are evaluated for the first time for these compounds. We calculate all the thermodynamic properties in a temperature range from 0 K to 1000 K and a pressure range from 0 GPa to 50 GPa, where the quasi-harmonic Debye model remains valid.

In the quasi-harmonic model, the nonequilibrium Gibbs function $G*(V;P,T)$ can be written as[22]

$$G*(V;P,T) = E(V) + PV + A_{\rm vib}(\Theta_{\rm D}(V);T),$$

where $E(V)$ is the total energy per unit cell, PV corresponds to the constant hydrostatic pressure condition, and $A_{\rm vib}(\Theta_{\rm D}(V);T)$ is the vibrational Helmholtz free energy which is given by

$$A_{\rm vib}(\Theta_{\rm D}(V);T) = nkT \times \left\{ \frac{9\Theta_{\rm D}}{8T} + 3\ln\left[1 - \exp(\Theta_{\rm D}/T) - D\left(\frac{\Theta_{\rm D}}{T}\right)\right]\right\},$$

where n is the number of atoms per formula unit, k is the Boltzmann constant, $D(\Theta_{\rm D}/T)$ is the Debye integral and $\Theta_{\rm D}$ represents the Debye temperature. The thermal equation of state $V(P,T)$ and the chemical potential $G(P,T)$ can be obtained by minimizing the nonequilibrium Gibbs function with respect to volume V. Other macroscopic properties as a function of pressure P and temperature T can also be derived from standard thermodynamic relations.[22]

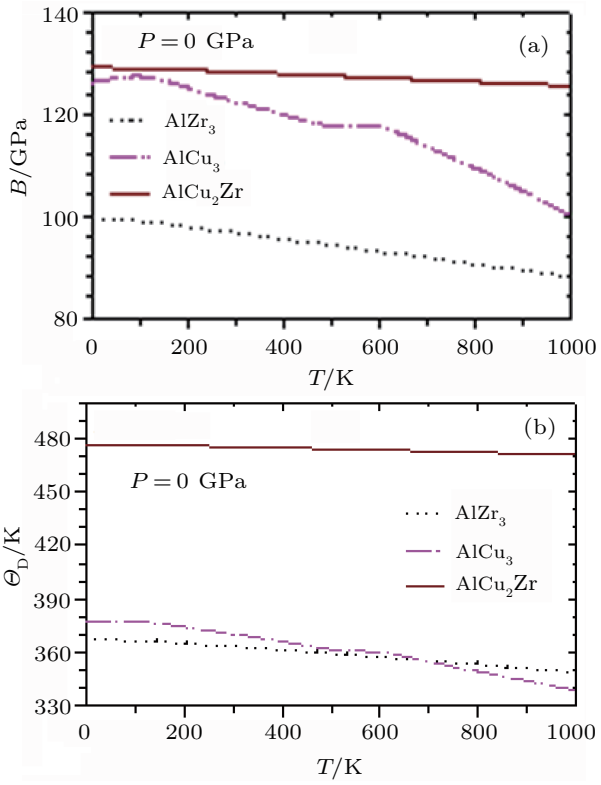


Fig. 6. (color online) Temperature dependences of (a) adiabatic bulk modulus and (b) Debye temperature of $AlZr_3$, $AlCu_3$, and $AlCu_2Zr$.

The temperature dependences of adiabatic bulk modulus, B of $AlZr_3$, $AlCu_3$, and $AlCu_2Zr$ alloys at $P = 0$ GPa are

shown in Fig. 6(a). Our calculations exhibit that B value for $AlCu_2Zr$ is nearly flat whereas for $AlZr_3$ compound, it decreases with temperature increasing up to 1000 K. We also note that in a temperature range of 0 K–600 K, B fluctuates for $AlCu_3$, it then decreases smoothly with temperature increasing until 1000 K. For $AlZr_3$, $AlCu_3$, and $AlCu_2Zr$ alloys, the values of B are found respectively to be 99 GPa, 126 GPa, and 129 GPa at $P = 0$ GPa and $T = 0$ K, which are in good agreement with the values computed using elastic constant data (Table 2).

Debye temperature is basically a measure of the vibrational response of the material. Debye temperature is not a strictly determined parameter; various estimates may be obtained through well-established empirical or semi-empirical formula, relating Θ_D to various macroscopic properties.[39] Figure 6(b) depicts the temperature dependences of Debye temperature, Θ_D of $AlZr_3$, $AlCu_3$, and $AlCu_2Zr$ compounds at zero pressure. Our calculated values of Θ_D using the quasi-harmonic Debye model are 367 K, 377 K, and 476 K, respectively for $AlZr_3$, $AlCu_3$, and $AlCu_2Zr$ alloys at zero pressure and zero temperature, which are in reasonable agreement with the values of 385 K, 381 K, and 397 K estimated using elastic constants data. These may be compared with the calculated value of Θ_D for Ni_3Al is 466 K.[12]

It is observed from Fig. 6(b) that Θ_D is the highest for $AlCu_2Zr$ and the lowest for $AlZr_3$ at zero temperature and pressure. The Debye temperatures decrease slowly with increasing temperature for $AlCu_2Zr$ and $AlZr_3$. But for $AlCu_3$, the Debye temperature decreases faster than those of the other two compounds. The temperature variations of all the phases reveal that there is a strong bonding in both the $AlCu_2Zr$ and $AlZr_3$ compounds where a weak bonding occurs in $AlCu_3$, which coincides with the DOS and elastic properties. This is due to the fact that the Debye temperature is related to the volume, V and adiabatic bulk modulus, B. The adiabatic bulk modulus B decreases and increases with increasing temperature and pressure, respectively but the volume, V, behaves in an opposite manner. It is found in Ref. [22] that B makes more contribution to the Debye temperature than, V. On the other hand, Debye temperature increases with increasing pressure (not shown).

The specific heat of the material is usually approximated by the contribution of the lattice specific heat. Figure 7 presents the estimated results on the temperature dependences of constant-pressure and constant-volume specific heat capacities C_P, C_V of $AlZr_3$, $AlCu_3$, and $AlCu_2Zr$ alloys. Due to the increase of temperature, phonon thermal softening occurs and hence heat capacities increase. The differences between C_P and C_V for $AlZr_3$, $AlCu_3$, and $AlCu_2Zr$ alloys are due to the thermal expansion caused by anharmonicity effects.[40] In the low temperature limit, the specific heat exhibits the Debye T^3 power-law behavior; at high temperature ($T > 300$ K), the anharmonic effect on heat capacity is suppressed, and C_V approaches the classical asymptotic limit $C_V = 3nNk_B = 99.7$ J/mol·K. These results exhibit the fact that the interactions between ions in $AlZr_3$, $AlCu_3$, and $AlCu_2Zr$ alloys have large effects on heat capacities especially at low temperatures. The calculations of Fatmi *et al.*[12] for a similar type of compound coincide with our results. To evaluate the electronic contribution to specific heat through the Sommerfeld constant, γ within the free electron model: $\gamma = (1/3)\pi^2 k_B^2 N(E_F)$, we can use $N(E_F)$ from the investigated DOS for the three alloys. This scheme gives the values 7.55, 2.95, and 21.93 mJ·mol^{-1}·K^{-2} for $AlZr_3$, $AlCu_3$, and $AlCu_2Zr$ alloys, respectively.

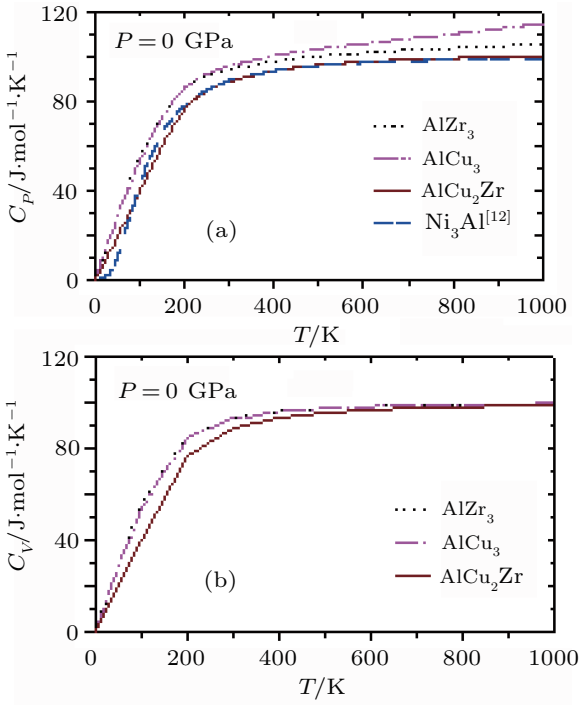


Fig. 7. (color online) Specific heats at constant (a) pressure and (b) volume versus temperature of $AlZr_3$, $AlCu_3$, and $AlCu_2Zr$.

Finally, the computed results on the variations of the volume thermal expansion coefficient, α_v with temperature and pressure for $AlZr_3$, $AlCu_3$, and $AlCu_2Zr$ alloys are displayed in Fig. 8. The volume thermal expansion coefficient, α_v reflects the temperature dependence of volume at constant pressure: $\alpha = (1/V)(dV/dT)_P$. Figure 8(a) depicts the temperature dependence of α_v at $P = 0$ GPa. The coefficient, α_v increases rapidly as the temperature increases up to $\sim$ 300 K and then gradually approaches towards a linear increase with temperature rising and the propensity of increment becomes moderate, which means that the temperature dependence of α_v is very small at high temperature. For a given temperature, the coefficient decreases drastically with the increase of pressure. The pressure dependence of α_v at 300 K is presented in Fig. 8(b). At high temperatures and high pressures, the thermal expansion would converge to a constant value. With

temperature rising, the average amplitude of atomic vibrations increases. For an anharmonic potential, it corresponds to the increase in the average value of inter-atomic separation, i.e., thermal expansion. The stronger the inter-atomic bonding, the smaller the thermal expansion is. The values of α_v are found to be 7.5×10^{-6} K^{-1}, 3.1×10^{-5} K^{-1}, and 5.3×10^{-5} K^{-1} for $AlCu_2Zr$, $AlZr_3$, and $AlCu_3$ alloys, respectively at $P = 0$ GPa and $T = 300$ K. The higher value of $AlCu_3$ indicates that it is softer than the other two compounds. For a given temperature, the coefficient α_v sharply decreases with the increase of pressure but for $AlCu_2Zr$, it is almost constant (see Fig. 8(b)). To date, there have been no experimental results nor other theoretical investigations for the thermal properties of $AlZr_3$, $AlCu_3$, and $AlCu_2Zr$ alloys; our investigations may serve as a guide for future research.

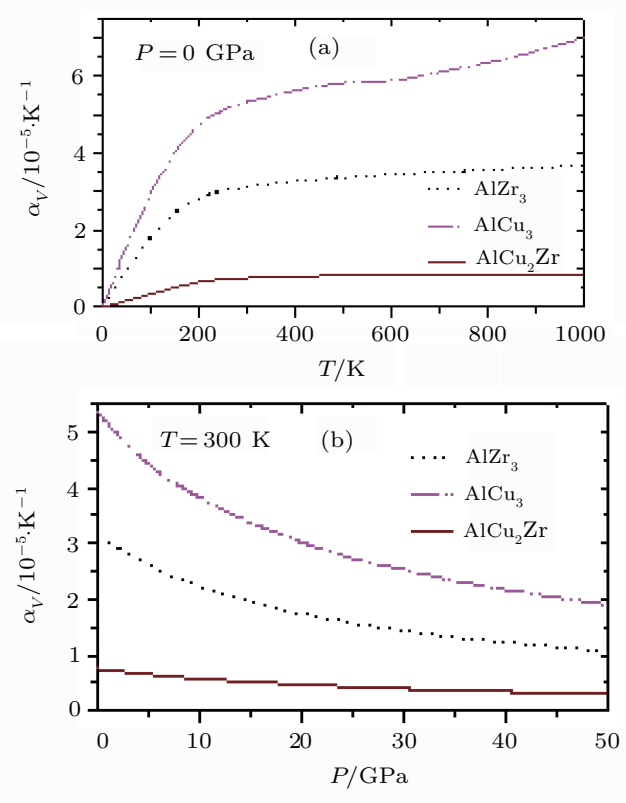


Fig. 8. (color online) Variations of α_v with (a) temperature and (b) pressure of $AlZr_3$, $AlCu_3$, and $AlCu_2Zr$.

The variations of entropy, S of $AlZr_3$, $AlCu_3$, and $AlCu_2Zr$ alloys each as a function of temperature and pressure are shown in Fig. 9. It is observed from Fig. 9(a) that at $P = 0$ GPa, S increases with increasing temperature. The rates of increase of entropy with temperature are almost the same for the compounds under study. This type of diagram is used in thermodynamics because it helps to visualize the heat transfer in the process. Entropy is a measure of how much the energies of atoms and molecules become more spread out in a process. Figure 9(b) shows that the entropy decreases with increasing pressure. This is due to the fact that when the pressure on the system increases, the volume decreases. The energies of the particles are in a smaller space, so they are less spread out. Hence the entropy decreases. It is observed from Fig. 9(b) that the rate of decrease of S is the largest for $AlCu_3$ and the smallest for $AlCu_2Zr$. Therefore the volume of $AlCu_3$ is more compressible than those of the other two Al-based alloys under the same pressure.

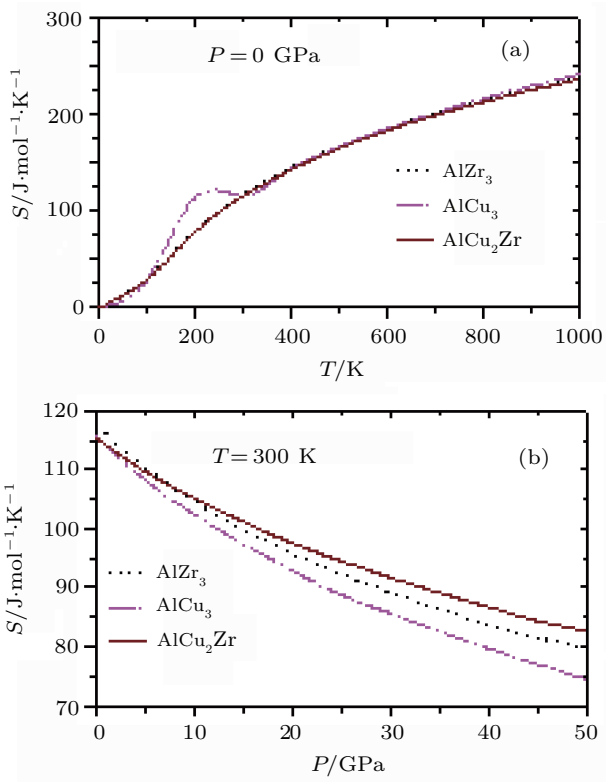


Fig. 9. (color online) Variations of $S$with (a) temperature and (b) pressure for $AlZr_3$, $AlCu_3$, and $AlCu_2Zr$.

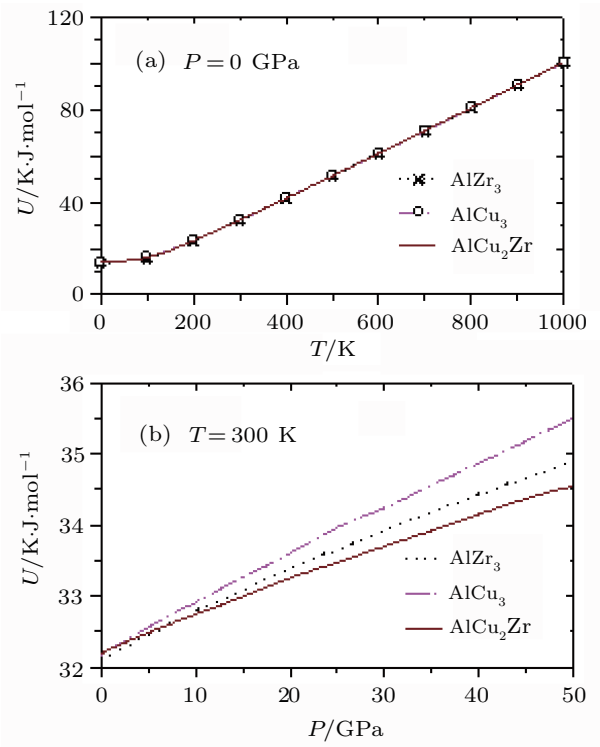


Fig. 10. (color online) (a) Temperature and (b) pressure dependences of U for $AlZr_3$, $AlCu_3$, and $AlCu_2Zr$.

The temperature and pressure variations of the calculated internal energies for $AlZr_3$, $AlCu_3$, and $AlCu_2Zr$ alloys are shown in Fig. 10. The internal energy is the energy associated with the random, disordered motions of molecules. It is observed from Figs. 10(a) and 10(b) that the internal energies increase with temperature and pressure increasing. At $P = 0$ GPa the rates of increase of U with temperature increasing are the same for all the compounds under study. On the other hand, at room temperature ($T = 300$ K), the internal energies increase 5.62%, 6.68%, and 4.72% for $AlZr_3$, $AlCu_3$, and $AlCu_2Zr$ alloys respectively, when the pressure changes from 0 GPa to 50 GPa.

3.5. Optical properties

The optical properties of $AlZr_3$, $AlCu_3$, and $AlCu_2Zr$ alloys may be derived from the knowledge of the complex dielectric function, $\varepsilon(\omega)$. Generally, there are two contributions for $\varepsilon(\omega)$, namely from intraband and interband transitions. The contribution from the latter is vital only for metals.[41] The complex dielectric function can be expressed as $\varepsilon(\omega) = \varepsilon_1(\omega) + i\varepsilon_2(\omega)$. The imaginary part $\varepsilon_2(\omega)$ is obtained from the momentum matrix elements between the occupied and unoccupied wave functions within the selection rules, whereas the real part $\varepsilon_1(\omega)$ of dielectric function can be derived from the imaginary part using the Kramers–Kronig relation. The knowledge of both $\varepsilon_1(\omega)$ and $\varepsilon_2(\omega)$ allows the calculation of important optical constants such as the refractive index $n(\omega)$, extinction coefficient $k(\omega)$, conductivity, optical reflectivity $R(\omega)$, absorption coefficient $\alpha(\omega)$, and energy-loss spectrum $L(\omega)$ using the expressions given in Ref. [42]. The calculational approaches are well established and widely available in the literature[43,44] and hence will not be repeated here.

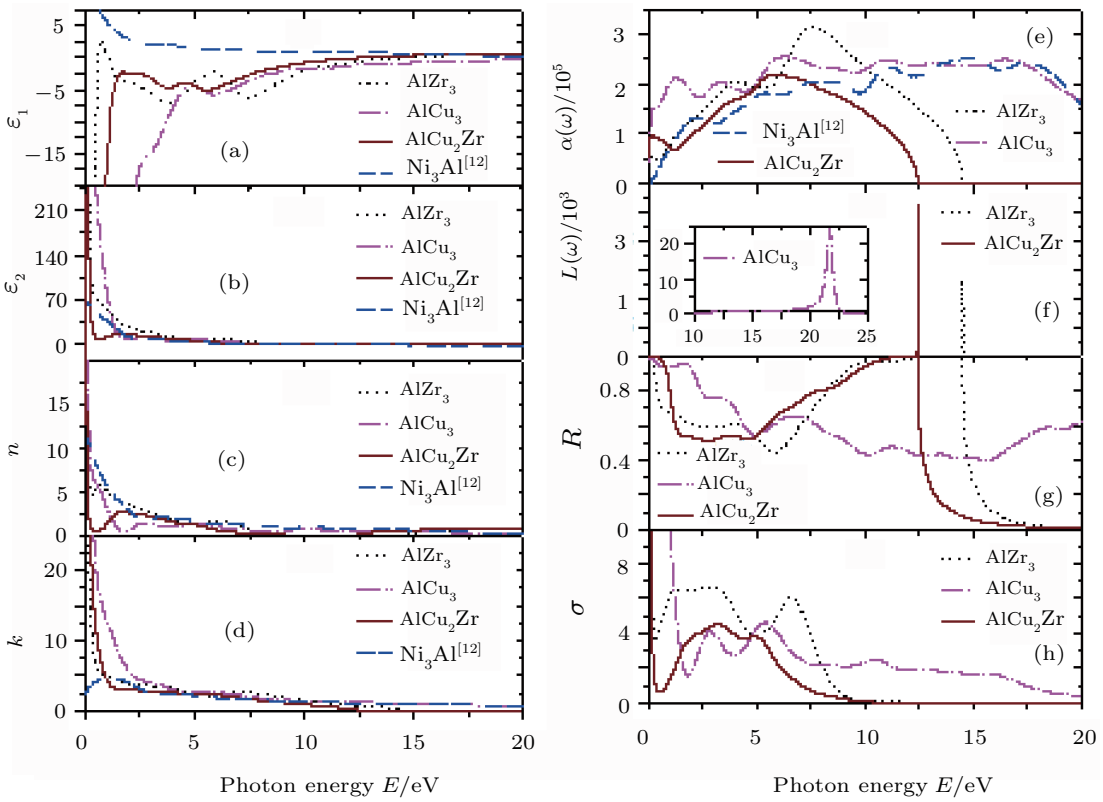


Fig. 11. (color online) (a) Real and (b) imaginary parts of dielectric function, (c) real and (d) imaginary parts of refractive index, (e) absorption, (f) loss function, (g) reflectivity, and (h) real part of conductivity of $AlZr_3$, $AlCu_3$, and $AlCu_2Zr$.

The estimated optical properties of $AlZr_3$, $AlCu_3$, and $AlCu_2Zr$ alloys at ground state are presented in Fig. 11, for the photon energy ranging from 0 eV up to 20 eV for polarization vector [100]. The available theoretical data for Ni_3Al[12] are also shown in the plots for comparison. Dielectric function is the most general property of a solid, which modifies the incident electromagnetic wave of light. Figures 11(a) and 11(b) show the real and imaginary parts of the dielectric function for $AlZr_3$, $AlCu_3$, and $AlCu_2Zr$ alloys along with the calculated values of Ni_3Al. Our results are similar to those for Ni_3Al.[12] The electronic band structure analysis shows that $AlZr_3$, $AlCu_3$, and $AlCu_2Zr$ alloys are metallic. Therefore, Drude term correction is required to include the effect of metallicity.[45,46]

The plasma frequencies of 10 eV, 4 eV, 6 eV, and damping values of 0.07 eV, 0.05 eV, 0.02 eV are used for $AlZr_3$, $AlCu_3$, and $AlCu_2Zr$ alloys, respectively. For all calculations, we use a 0.5-eV Gaussian smearing. The real part ε_1 goes through zero from below about 14.52 eV, 21.66 eV, 12.47 eV and the imaginary part ε_2 approaches zero damping values

of 14.98 eV, 22.80 eV, and 12.98 eV for $AlZr_3$, $AlCu_3$, and $AlCu_2Zr$ alloys, respectively. Metallic reflectance characteristics are exhibited in the range $\varepsilon_1 < 0$.

The velocity of propagation of an electromagnetic wave through a solid is given by the frequency dependent complex refractive index $N = n + ik$, where the real part n is related to the velocity and the imaginary part k, the extinction coefficient is related to the decay or damping of the oscillation amplitude of the incident electric field. The refractive indexes and extinction coefficients are illustrated in Figs. 11(c) and 11(d). The static refractive index $n(0)$ is found to have the values 11.8 ($AlCu_3$), 19.3 ($AlZr_3$), and 12.4 ($AlCu_2Zr$), which agrees well with that of another Al-based intermetallic compound Ni_3Al (14.56).[12] The values of extinction coefficients, k each show a maximum value at 0.0 eV, then they decrease rapidly and turn to zero at about 15.0 eV, 22.96 eV, and 12.43 eV for $AlZr_3$, $AlCu_3$, and $AlCu_2Zr$ alloys, respectively.

Figure 11(e) shows the absorption coefficient spectra of the $AlZr_3$, $AlCu_3$, and $AlCu_2Zr$ alloys, which begin at zero photon energy due to their metallic nature. In Fig. 11(e), we show the absorption coefficient spectrum with one peak between 0.78 eV and 5.73 eV for $AlZr_3$ which rises and then decreases rapidly in the high-energy region. Nearly the same features can be seen for $AlCu_3$ and $AlCu_2Zr$ but with two prominent peaks for $AlCu_3$. The highest peaks appear at 7.55 eV, 6.26 eV, and 5.80 eV for $AlZr_3$, $AlCu_3$, and $AlCu_2Zr$ alloys, respectively. The absorption coefficient spectrum of Ni_3Al is also shown in Fig. 11(e) for comparison, for which the highest peak occurs at 14.93 eV.[12] It is observed from the figure that at higher photon energies, Ni_3Al and $AlCu_3$ have roughly similar absorption coefficient spectra.

Loss function is intimately related to absorption and reflection. Loss function refers to the fast electron traversing in a material. It is clear from the study of the figure that maximum reflectivity occurs where the minimum absorption takes place. So the study of loss function is the most important in material study. The electron energy loss function $L(\omega)$ is depicted in Fig. 11(f). The peaks in $L(\omega)$ spectra represent the characteristics associated with the plasma resonance and the corresponding frequency is the so-called plasma frequency, ω_P,[47] which occurs at $\varepsilon_2 < 1$ and $\varepsilon_1 = 0$.[46,48] The peaks of $L(\omega)$ located at 14.5 eV, 21.7 eV, and 12.4 eV correspond to plasma frequencies of $AlZr_3$, $AlCu_3$, and $AlCu_2Zr$ alloys, respectively. Further, these peaks correspond to irregular edges in the reflectivity spectra (Fig. 11(g)), and hence an abrupt reduction occurs at each of these peak values in the reflectivity spectra. If the incident light has frequency greater than the plasma frequencies of the alloys under study, these alloys will be transparent and will change from metallic to dielectric response.

The variations of calculated optical reflectivity $R(\omega)$ with incident photon energy are displayed in Fig. 11(g). It is observed from the figure that $AlZr_3$ and $AlCu_2Zr$ have their maximum reflectivity values ($\sim$100%) in the infra-red region as well as in the ultra-violet region. On the other hand, $AlCu_3$ has maximum reflectivity only in the infra-red region. Again in the visible light region (energy range $\sim$1.8 eV–3.1 eV), it is observed from Fig. 11(g) that $AlCu_3$ has larger reflectivity than those of the $AlZr_3$ and $AlCu_2Zr$ alloys, but all of them have reflectivities more than 44%. This indicates that the capability of $AlCu_3$ to reflect visible light is stronger than those of the other two alloys. On the other hand, $AlZr_3$ and $AlCu_2Zr$ alloys are better reflectors than that of the $AlCu_3$ alloy in the ultra-violet region. According to Li *et al.*,[45] a MAX-phase compound will be capable of reducing solar heating if it has a reflectivity of $\sim$ 44% in the visible light region. Hence, we may conclude that all the compounds under study are also candidate materials for coating to reduce solar heating.

For the three alloys, their photoconductivities start with zero photon energy (Fig. 11(h)). This indicates that the materials have no band gap that is evident from band structure calculations (Fig. 2). Moreover, the photoconductivities and hence electrical conductivities of these materials increase as a result of absorbing photons. From Fig. 11(h), we observe that the maximum optical conductivities occur at energy 2.72 eV for $AlZr_3$, 5.40 eV for $AlCu_3$, and 3.21 eV for $AlCu_2Zr$ within the energy range of 2 eV to 6.84 eV, respectively. This implies that $AlCu_3$ will be more highly electrically conductive than the other two alloys when the incident radiation has an energy within this range. The photoconductivities reach zero at about 10 eV for both the compounds $AlZr_3$ and $AlCu_2Zr$; $AlCu_3$ also reaches zero but at 22.5 eV (not shown). There is a photoconductivity for none of the phases when the photon energy is higher than 22.5 eV. We are not aware of any other theoretical calculations or experimental data for the optical properties of $AlZr_3$, $AlCu_3$, and $AlCu_2Zr$ alloys. Thus, our results would provide a useful reference for further investigations.

4. Conclusions

First-principles calculations based on DFT and the quasi-harmonic Debye model are used to investigate different properties of $AlZr_3$, $AlCu_3$, and $AlCu_2Zr$ alloys. Based on the calculated results, we find that $AlZr_3$ phase has the highest stiffness among the three phases. On the other hand, the Poisson's ratio changes from 0.264 to 0.341, which indicates that AlM_3 (M = Zr and Cu) and $AlCu_2Zr$ compounds show metallic behaviors. In view of Pugh's criterion for these three alloys it is observed that these three compounds show ductility behavior. Under the effect of pressure, the value of C_{11} increases rapidly with pressure compared to C_{12} and C_{44} for all compounds, which indicates that the longitudinal strain produces a significant change in volume. The larger Poisson's ratio of

$AlCu_3$ compared to those of the other two phases indicates better plasticity.

It is also observed from the DOS value that $AlZr_3$ has a more stable structure than the other two alloys. The pseudo-gap around the Fermi level indicates the presence of the directional covalent bonding. The $AlCu_3$ and $AlZr_3$ show hole-like Fermi surface whereas $AlCu_2Zr$ shows both electron-like and hole-like Fermi surface. The stronger the inter-atomic bonding, the smaller the thermal expansion is. The smaller value of $AlCu_2Zr$ indicates stronger atomic bonding whereas the higher value of $AlCu_3$ indicates that it is softer than the other two compounds. The reflectivities of these compounds are high ($\sim$100%) in the IR as well as in the UV region. In the visible region, all the compounds under study may be considered as potential coating materials to avoid solar heating.

References

[1] Sauthoff G, Westbrook J H and Fleischer R L (eds.) 1994 *Intermetallic Compounds* (New York: Wiley) **1** 991
[2] Cahn R W 1998 *Intermetallics* **6** 563
[3] Rajagopalan P K, Sharma I G and Krishnan T S 1999 *J. Alloys Compd.* **285** 212
[4] Zhou W, Liu L J, Li B L, Song Q G and Wu P 2009 *J. Electron. Mater.* **38** 356
[5] Emmanuel C and Sanchez J M 2002 *Phys. Rev. B* **65** 094105
[6] Ghosh G and Asta M 2005 *Acta Mater.* **53** 3225
[7] Ghosh G 2007 *Acta Mater.* **55** 3347
[8] Ma W J, Wang Y R, Wei B C and Sun Y F 2007 *Trans. Nonferrous Met. Soc. China* **17** 929
[9] Pauly S, Das J, Mattern N, Kim D H and Eckert J 2009 *Intermetallics* **17** 453
[10] Guan Y Z, Zhang H Y and Li W 2011 *Physica B* **406** 1149
[11] Zhang B R, Jia Z, Duan X Z and Yang X Z 2013 *Acta Phys. Polonica A* **23** 668
[12] Fatmi M, Ghebouli M A, Ghebouli B, Chihi T, Boucetta S and Heiba Z K 2011 *Rom. J. Phys.* **56** 935
[13] Clark S J, Segall M D, Probert M J, Pickard C J, Hasnip P J and Payne M C 2005 *Z. Kristallogr.* **220** 567
[14] Materials Studio CASTEP manual 2010 ©Accelrys 2010, p. 261 http://www.tcm.phy.cam.ac.uk/castep/documentation/WebHelp/CASTEP.html
[15] Hohenberg P and Kohn W 1964 *Phys. Rev.* **136** 864
[16] Perdew J P, Ruzsinszky A, Csonka G I, Vydrov O A, Scuseria G E, Constantin L A, Zhou X and Burke K 2008 *Phys. Rev. Lett.* **100** 136406
[17] Vanderbilt D 1990 *Phys. Rev. B* **41** 7892
[18] Head J D and Zerner M C 1985 *Chem. Phys. Lett.* **122** 264
[19] Brillouin C R and Hebd C R 1930 *Seances. Acad. Sci.* **191** 292
[20] Monkhorst H J and Pack J D 1976 *Phys. Rev. B* **13** 5188
[21] Milman V and Warren M C 2001 *J. Phys.: Condens. Matter* **13** 241
[22] Blanco M A, Francisco E and Luaña V 2004 *Comput. Phys. Commun.* **158** 57
[23] Blanco M A, Penda's A M, Francisco E, Recio J M, Franco R and Mol J 1996 *Struct. Theochem.* **368** 245
[24] Flórez M, Recio J M, Francisco E, Blanco M A and Pendás A M 2002 *Phys. Rev. B* **66** 144112
[25] Francisco E, Recio J M, Blanco M A and Pendás A M 1998 *J. Phys. Chem.* **102** 1595
[26] Birch F 1978 *J. Geophys. Res.* **83** 1257
[27] Meng W J, Faber J Jr, Okamoto P R, Rehn L E, Kestel B J and Hitterman R L 1990 *J. Appl. Phys.* **67** 1312
[28] Draissia M, Debili M Y, Boukhris N, Zadam M and Lallouche S 2007 *Copper* **10** 65
[29] Meyer Z U, Reckendorf R, Schmidt P C and Weiss A Z 1989 *Phys. Chem. N F* **163** 103
[30] Mattesini M, Ahuja R and Johansson B 2003 *Phys. Rev. B* **68** 184108
[31] Haines J, Leger J M and Bocquillon G 2001 *Ann. Rev. Mater. Res.* **3** 1
[32] Pugh S F 1954 *Philos. Mag.* **45** 823
[33] Zener C M 1948 *Elasticity and Anelasticity of Metals* (Chicago: University of Chicago Press)
[34] Chen P, Li D L, Yi J X, Li W, Tang B Y and Peng L M 2009 *Solid State Sci.* **11** 2156
[35] Xu J H, Lin W and Freeman A J 1993 *Phys. Rev. B* **48** 4276
[36] Xu J H, Oguchi T and Freeman A J 1987 *Phys. Rev. B* **36** 4186
[37] Hong T, Watson-Yang T J, Freeman A J, Oguchi T and Xu J H 1990 *Phys. Rev. B* **41** 12462
[38] Swetarekha Ram, Kanchana V, Svane A, Dugdale S B and Christensen N E 2013 *J. Phys.: Condens. Matter* **25** 155501
[39] Leadbetter H M, Reep R P and Clark A F (eds.) *Materials at Lower Temperature* 1983 (Ohio: ASM Metal Park)
[40] Ali M S, Islam A K M A, Hossain M M and Parvin F 2012 *Physica B* **407** 4221
[41] Reshak A H, Atuchin V V, Auluck S and Kityk I V 2008 *J. Phys.: Condens. Matter* **20** 325234
[42] Shaha S, Sinha T P and Mookarjee A 2000 *Phys. Rev. B* **62** 8828
[43] Li C, Wang B, Li Y and Wang R 2009 *J. Phys. D: Appl. Phys.* **42** 065407
[44] Li C, Kuo J, Wang B, Li Y and Wang R 2009 *J. Phys. D: Appl. Phys.* **42** 075404
[45] Li S, Ahuja R, Barsoum M W, Jena P and Johansson B 2008 *Appl. Phys. Lett.* **92** 221907
[46] Saniz R, Ye L H, Shishidou T and Freeman A J 2006 *Phys. Rev. B* **74** 014209
[47] Fox M 1972 *Optical Properties of Solids* (New York: Academic Press)
[48] De Almeida J S and Ahuja R 2006 *Phys. Rev. B* **73** 165102